SUBSTITUENT EFFECTS ON THE ABSORPTION
AND VIBRATIONAL SPECTRA OF SOME 2-HYDROXY
SCHIFF BASES: DFT/TDDFT, NATURAL BOND
ORBITAL AND EXPERIMENTAL STUDY

S. A. Elroby[1,3], S. Aboud[1], S. G. Aziz[1],   UDC 541.65:548.737
and R. Hilal[1,2]

The electronic structure of salicylideneaniline (SA) and some of its derivatives are investigated both experimentally and theoretically. The equilibrium geometric structures of the studied compounds are determined at the B3LYP/6-311++G** level of theory. A set of 12 substituted SA derivatives is considered in the present work. The choice of these substituents aims to create a push-pull system on the SA basic structure which would shade light onto its photo physics. The electronic absorption spectra of SA are recorded in the UV-VIS region, in both polar and nonpolar solvents. Assignments of the observed electronic transitions are facilitated via time-dependent density functional theory (TDDFT) computations at the same level of theory. Electronic configurations contributing to each excited state are identified and the relevant MOs are characterized. The extent of delocalization and intramolecular charge transfer are estimated and discussed in terms of natural bond orbitals (NBO) analysis and second order perturbation interactions between donor and acceptor MOs. Solvent effects on the electronic absorption spectra are discussed in terms of the difference in polarizabilities of the ground and excited states. FTIR spectra of SA and its derivatives are measured in KBr platelets. Detailed vibrational assignments are given based on the calculated potential energy distributions. "IR marker bands" that characterize the SA framework are identified. The effect of substituents, the nature of the characteristic "marker bands", and intensity quenching of some bands are discussed.

DOI: 10.1134/S0022476615030038

Keywords: electronic spectra, vibrational spectra, DFT/TDDFT, solvent and substituent effects, NBO analysis, 2-hydroxy Schiff bases.

INTRODUCTION

Aromatic Schiff bases have been [1-4] and still are the subject of numerous studies because of possible applications, e.g. in molecular memories and switches [5-7]. This class of molecular systems is of fundamental interest because it shows two interesting phenomena, namely, the excited state intramolecular proton transfer (ESIPT) and photochromism. The best

---

[1]Chemistry Department, Faculty of Science, King Abdullaziz University, Jeddah, Saudi Arabia. [2]Chemistry Department, Faculty of Science, Cairo University, Giza, Egypt; rhilal@kau.edu.sa. [3]Chemistry Department, Faculty of Science, Benisuef University, Benisuef, Egypt. The text was submitted by the authors in English. *Zhurnal Strukturnoi Khimii*, Vol. 56, No. 3, pp. 444-456, May-June, 2015. Original article submitted March 05, 2014.

known photochromic Schiff base is salicylideneaniline (SA). This molecule and its derivatives have been widely studied over a wide span of time [8-24]. In SA and its derivatives, the intramolecular hydrogen bonding opens a possibility of fast proton transfer between different tautomers followed by isomerization changes, leading to a metastable photochromic modification of the initial structure. Numerous experimental studies [25-28] on SA have been devoted to the analysis of the mechanism and dynamics of the proton transfer reaction from the primary excited enol form to the keto tautomer and the creation of the photochromic tautomer in the ground electronic state. Nevertheless, the results are not fully consistent and much controversy is still present.

The absorption spectrum of SA shows a quite prominent band at 300-400 nm attributed to the photoexcitation to a $\pi\pi^*$ excited state [29]. The fluorescence spectrum also presents a single largely Stokes shifted band centered at around 570 nm. This band is believed to come from the *cis*-keto tautomer and is also a $\pi\pi^*$ state. The quantum yield of the fluorescence is quite low [24]. A global picture of photochromism in SA has been reached based on the time- resolved experiments [24, 29]. This picture starts with photoexcitation to the $\pi\pi^*$ excited state followed by a quick transfer of the hydroxylic proton to the nitrogen imino atom resulting in the fluorescent *cis*-keto tautomer. This species is the precursor of the photochromic transient, believed to be a ground state keto tautomer. This transient has a long lifetime of the order of milliseconds and a maximum absorption band at 474 nm [24]. However, the detailed mechanism about the species involved in the whole process and the time of the different steps is not a settled question. In fact, several different decay mechanisms have been proposed, namely, thermal deactivation and internal conversion (IC) through conical intersections (CIs) or intersystem crossing.

The present work attempts to provide a detailed experimental and quantum chemical study of the electronic and vibrational spectra of SA at high level DFT and TDDFT methods. The origin of each absorption band is identified and the contributing configurations and MOs are characterized. The magnitude and direction of the intramolecular charge transfer is also identified and evaluated. In this respect, natural bond orbital analysis (NBO) is carried out to identify the extent of delocalization and the charge transfer of the electron density in the studied molecular systems. The effect of substituents on the vibrational spectra is also investigated. An attempt is made to identify and assign the "IR marker bands" for SA. Solvent and substituent effects are quantitatively analyzed and discussed.

EXPERIMENTAL

Compounds. SA and its derivatives were prepared by conventional methods where equimolar quantities of aniline and salicylaldehyde were heated in spectroscopically pure dry ethanol and then the solution was allowed to cool. Compounds were then recrystallized from chloroform.

Solvents. Spectroscopic-grade solvents (Merck) were used without any further purification.

Measurements. Infrared spectra of the compounds were recorded on a Shimad24 820/PC FT-IR spectrometer within the range 4000-400 cm^{-1}. For samples in the solid state, the IR spectra were measured in KBr pellets at a resolution of 1 cm^{-1}. All UV-VIS spectral measurements were carried out using a Perkin–Elmer UV-Visible spectrophotometer (model Lambda 2).

Computational methods. All computations were carried out using the Gaussian 09W software package [30]. Molecular geometries of all of the studied compounds were fully optimized using the 6-311++G** basis set using Beck's three-parameter-hybrid (B3LYP) DFT method [31-33]. No symmetry constrains were applied during the geometry optimization. Calculations of the electronic spectra and excited states were carried out at the TDDFT/6-311++G** level of theory [34]. The choice of this basis set was due to its flexibility, and the fact that diffuse *p* functions on the hydrogen atoms tend to compensate the anharmonic effects of the CH and NH stretches. The force constants were analytically computed at the fully optimized geometries. NBO calculations have been performed at the B3LYP/6-311+G** level using the NBO 3.1 program as implemented in the Gaussian09W software package in order to quantitatively measure the intramolecular delocalization in the studied systems. NBO theory [35, 36] proved to be extremely useful in analyzing hyper conjugative [37] interactions through the second-order perturbation energy ($E^{(2)}$), which is estimated as

415

$$E^{(2)} = \Delta E_{ij} = q_i (F_{ij})^2/\Delta\square,$$

where q_i is the donor orbital occupancy, $\Delta\square$ is the difference between the energy of an acceptor orbital (j) and a donor orbital (i), and F_{ij} is the off-diagonal NBO Kohn–Sham matrix. Throughout this work MOs were constructed using the Gauss View 5.0.8 visualization program [38].

RESULTS AND DISCUSSION

Electronic and vibrational spectra of SA. Scheme 1 displays the equilibrium geometric structure and the numbering system of SA adopted in the present work.
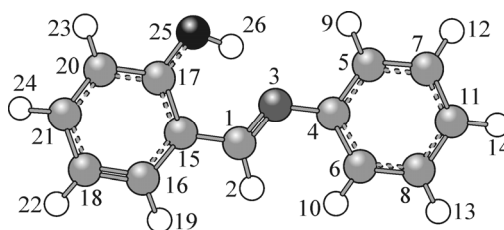
Scheme 1. Equilibrium geometric structure and atom labeling of SA adopted in the present work.

Fig. 1 displays the electronic absorption spectrum of SA in cyclohexane and ethanol as solvents. The spectrum is composed of low intensity diffuse bands. One can identify five overlapping bands and a shoulder, spanning the 350-200 nm range. An increase in the solvent polarity causes a marked blue shift of all observed transition bands. Table 1 presents the electronic spectral characteristics of SA in both polar and nonpolar solvents. It is instructive at this point to identify the origin of these observed transition bands. A comparison between the observed and theoretically computed spectra is given in Table 1. The correspondence is excellent. The first transition which is predicted at 353 nm (observed 350 nm) is composed of two main configurations: 51→53 (–0.18) and 52→53 (0.68). MOs involved in these two configurations are displayed in Fig. 2. Three MOs involved are the delocalized π orbitals, and hence, the respective transition band corresponds to a typical ππ* state. The second transition appears as a diffuse overlapping band observed at 322 nm. This transition is not predicted theoretically for the *trans*-enol structure.

The third transition is observed at 305 and is predicted theoretically at 304 nm. The same two configurations 51→53 (0.67) and 52→53 (0.19) contribute to the S_3 state indicating its ππ* nature. The fourth band is observed in the 280-270 nm range and is predicted theoretically at 282 nm. There is only one configuration contributing to the S_4 state. This configuration is 49→53 (0.70). MO 49 is localized completely on the *N*-phenyl moiety, whereas vacant MO 53 is a delocalized orbital.
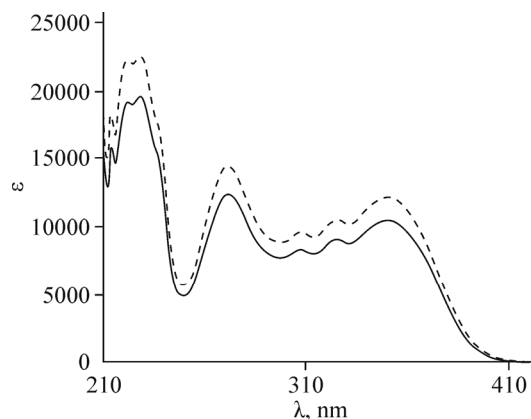

Fig. 1. Electronic absorption spectra of SA, in (–) cyclohexane and (– – –) ethanol as solvents.

TABLE 1. Experimentally Observed and Theoretically Predicted Spectral Characteristics of SA

Observed λ, nm		Theoretically predicted for SA enol				Theoretically predicted for SA *cis*-keto			
Cyclohexane	Methanol	E, eV	λ, nm	f	Contribution	E, eV	λ, nm	f	Contribution
						2.96	419	0.3	52-53 (0.77)
						3.21	386	0.0	51-53 (0.70)
353	345	3.51	353	0.4	51-53 (0.18) 52-53 (0.68)				
322	327					3.91	317	0.4	50-53 (0.70)
305	300	4.07	305	0.5	51-53 (0.67) 52-53 (0.19)	4.18	297	0.0	49-53 (0.22) 42-54 (0.66)
		4.26	291	0.0	49-53 (0.70)				
270	283	4.40	282	0.0	50-53 (0.63) 51-5 (0.13) 52-54 (0.27)	4.56	271	0.01	49-53 (0.63) 50-54 (–0.17)
240	249	4.92	252	0.0	48-53 (0.44) 52-54 (0.36)	4.75	262	0.1	48-53 (0.22) 52-55 (0.66)
		5.00	248	0.1	48-53 (0.32) 52-54 (0.52) 50-53 (0.24)				
227									

Therefore, the S_4 state is ππ* involving a considerable charge transfer character. This charge transfer takes place against the dipole moment vector, and consequently, the corresponding excited state S_4 has a lower dipole moment, and hence, is much less polarized. This would suggest that polar solvents stabilize the more polar ground state to a greater extent and thus cause
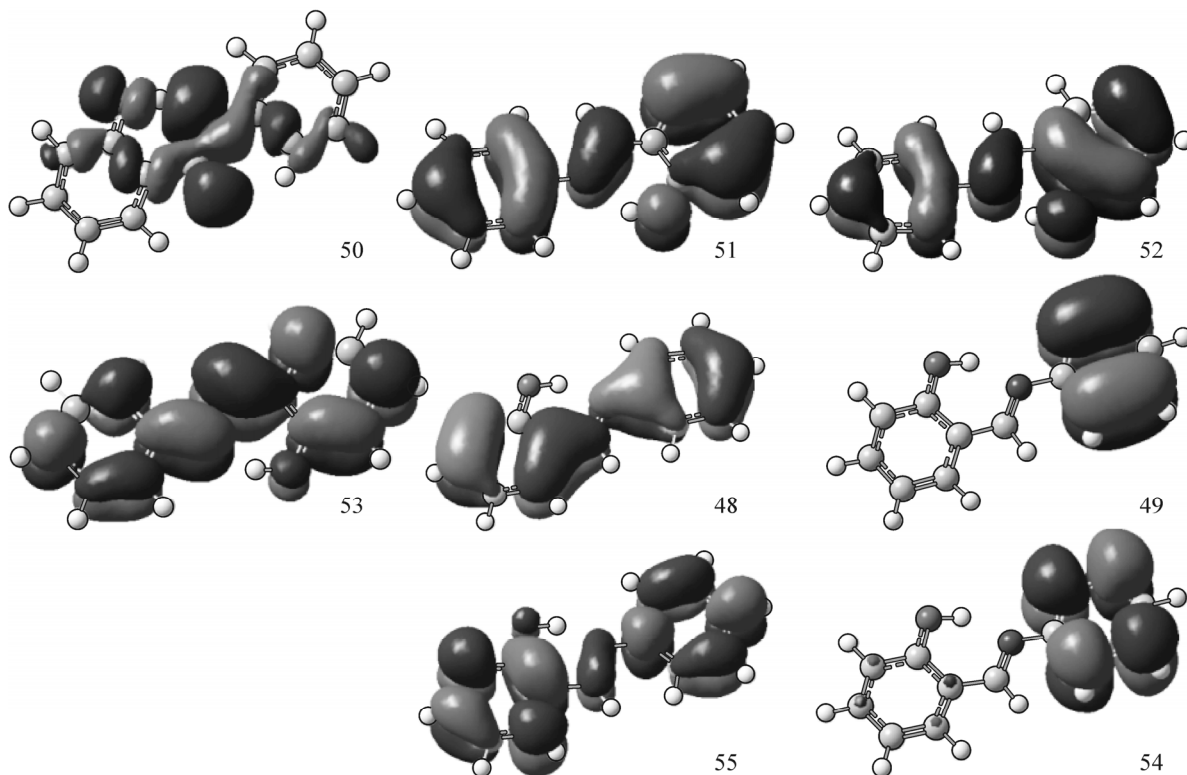
Fig. 2. MOs involved in the electronic states of SA (52 and 53 represent HOMO and LUMO, respectively).

a red shift of the observed band maxima. The fifth excited state S_5 is observed at 249 nm and predicted theoretically at 252 nm. The correspondence is excellent.

An increase in the solvent polarity has but little effect on the spectrum of SA. Thus, the first absorption band suffers a blue shift of 8 nm whilst the second band suffers a red shift by almost the same amount. This increases the overlap between the two bands. This small solvent effect is expected in view of the similar polarities of both ground and excited states for these two transitions. Furthermore, there seems to be a general trend of enhancing intensity with increasing solvent polarity. Table 1 presents a comparison between the experimentally observed and theoretically computed spectral characteristics of SA.

Although the present high level TDDFT calculations are able to predict well all the observed transitions, yet the second 322 nm band is not predicted theoretically at all. This might suggest the presence of another absorbing species in the solution, presumably a *cis*-keto form of SA. Table 1 displays the computed spectral band positions and intensities of the *cis*-keto form of SA. This form seems to have long wavelength ππ* absorption bands at 418 nm which are not observed in the experimental spectra. The second S2 transition predicted theoretically at 317 nm is in good correspondence with the observed 322 nm band. However, the correspondence in the short wavelength region seems much less satisfactory than that of the enol form.

The present study focuses on the effect of substituents on the electronic and vibrational spectra of SA. In order to fulfill this goal it is instructive to analyze and discuss the NBO results for SA. The NBO analysis provides the electron density distribution on atoms and in bonding regions. By comparing a set of molecules you can, for instance, see the donor or acceptor effect of the substituent. Table 2 presents the most relevant perturbation interactions within the natural orbitals of SA. In this table, the reported relevant interaction values are ≥10 kcal/mol. Careful inspections of the data in this table reveals that:

1. The C–N π orbital interacts equally well with both phenyl rings. In fact, its interaction with the OH–Ph ring is greater. Furthermore, the lone pair orbital of the nitrogen atom enjoys hyperconjugation with the C_1–H_2 orbital.

2. The oxygen lone pair orbital, on the other hand, interacts essentially with the π framework of the phenyl ring. The interaction of the oxygen atom lone pair orbitals with the hydrogen virtual and Rydberg orbitals is pronounced.

3. It is surprising to notice a decrease in the population of the NBO C_{15}–C_{17}, C_{16}–C_{18}, and C_{20}–C_{21} reflecting a charge transfer away from the phenyl ring. This is also evident in the case of the population of the oxygen lone orbital LP(3), which is reduced by almost 0.5 e.

In conclusion, SA enjoys the linear conjugation that is responsible for the observed spectrum. No specific part of the molecule manifests itself in the observed spectrum due to the extended π system. The interaction between the oxygen and hydrogen atomic orbitals is of a covalent character, and thus, a proton transfer toward the nitrogen atom would be opposed by a high energy barrier.

It would be reasonable at this point to analyze and discuss the vibrational spectrum of SA. Fig. 3 displays the FTIR spectrum of SA measured as a KBr pellet. The spectrum is composed of three main regions. A broad low intensity envelope spans the 3600-3200 cm^{-1} range. This envelope encloses the aromatic symmetric and asymmetric CH stretching and OH stretching modes. The middle region is of much higher intensity and is composed of several intense sharp absorption peaks corresponding to the aromatic ring vibration and the C=N stretching mode that can be identified at 1613 cm^{-1}. The third region spans the 1000-500 cm^{-1} range and is composed of several sharp peaks of variable intensities corresponding to the coupling and combination bands.

A comparison of the experimentally observed and theoretically computed vibrational bands is given in Table 4 along with their assignments. In the present discussion, we select one band from each of the three regions. The selected bands correspond to the main functional groups characterizing the SA framework, namely, OH, C=N, and the aromatic ring where substituents will be introduced. Thus, in this part and the subsequent discussion, we focus on three bands which can be considered as "IR marker bands" for SA. These are the OH stretching predicted as strong (relative intensity 334) at 3175 cm^{-1}, the C=N stretching and coupling vibrational band of the C=N vibrational mode, which is observed and predicted in the 1600 cm^{-1} region, and the phenyl ring breathing modes observed at 750 cm^{-1} and predicted at 860 cm^{-1}.

| Compound	Donor orbital	Acceptor orbital	$E^{(2)}$, kcal/mol	NBO	Population
SA	C1–N3	*C4–C5	13.68	C15–C17	1.5666
	C4–C5	*C1–N3	15.15	C16–C18	1.7081
	C15–C17	*C1–N3	22.61	C20–C21	1.6965
	LP(1) N3	*C1–H2	11.62	LP(1)N3	1.8643
	LP(2)O25	*C15–C17	37.10	LP(2)O25	1.8103
	*C1–N3	*C4–C5	47.59	LP(3)O25	1.5647
	*C1–N3	*C15–C17	136.02		
	C17–O25	*H26	17.84		
	LP(3)O25	*H26	456.60		
o-NO$_2$	C14–C15	*C1–N3	25.91	C4–C5	1.6227
	*C1–N3	*C14–C15	139.93	C6–C9	1.6625
	C16–O24	*H25	17.50	C14–C15	1.6352
	LP(1)N3	*H25	32.53	C16–C19	1.5893
	LP(1)O24	*H25	15.03	C17–C20	1.6225
	LP(3)O24	*H25	475.69	LP(3)O24	1.4371
p-NO$_2$	C1–N3	C4–C6	10.78	C4–C6	1.60999
	C1–N3	C14–C15	7.09	C5–C7	1.6669
	C4–C6	*C1–N3	7.77	C9–C11	1.6438
	C14–C15	*C1–N3	26.18	C5–C7	1.6669
	LP(1)N3	*C1–H2	10.99	C9–C11	1.6437
	LP(2)O24	*C16–C19	35.87	C14–C15	1.6305
	*C1–N3	*C4–C6	92.72	C17–C20	1.6158
	*C1–N3	*C14–C15	124.98	LP(3)O24	1.5532
	C16–O24	*H25	17.51		
o-OCH$_3$	C1–N3	*C4–C6	15.25	C4–C6	1.6197
	C4–C6	*C1–N3	10.61	C5–C7	1.6759
	C12–C14	*C1–N3	22.09	C–8–C9	1.6712
	LP(2)O22	*C12–C14	37.00	C17–C18	1.6991
	*C1–N3	*C4–C6	131.01	LP(3)O22	1.5696
p-OCH$_3$	C1–N3	*C4–C5	10.43	C4–C5	1.6429
	C4–C5	*C1–N3	11.75	C6–C9	1.7209
	C14–C16	*C1–N3	21.70	C7–C11	1.6562
	LP(1)N3	*C1–H2	11.31	C14–C16	1.5717
	LP(2)O24	*C14–C16	16.50	C15–C17	1.7062
	*C1–N3	*C4–C5	45.49	C19–C20	1.6969
	*C1–N3	*C14–C16	172.86	LP(3)O24	1.5616
	C16–C24	*LPH25	17.63		
	LP(1)N3	*LPH25	37.18		
	LP(1)O24	*LPH25	14.4		
	LP(3)O24	LP(1)H25	459.78		

Substituent effect. The substituted SA derivatives studied in the present work are presented in Scheme 2. Two sets of substituents have been considered. A set of electron withdrawing substituents, namely –Cl, –Br, and –NO$_2$ substituted in the *ortho*- and *para*-positions of the N–Ph moiety. Another set is composed of three electron donating substituents, namely, –OH, –NH$_2$, and –OCH$_3$ also substituted in both *ortho*- and *para*-positions. The choice of these substituents aims to create a push-pull system on the SA basic structure, which hopefully would shade light onto its photo physics.
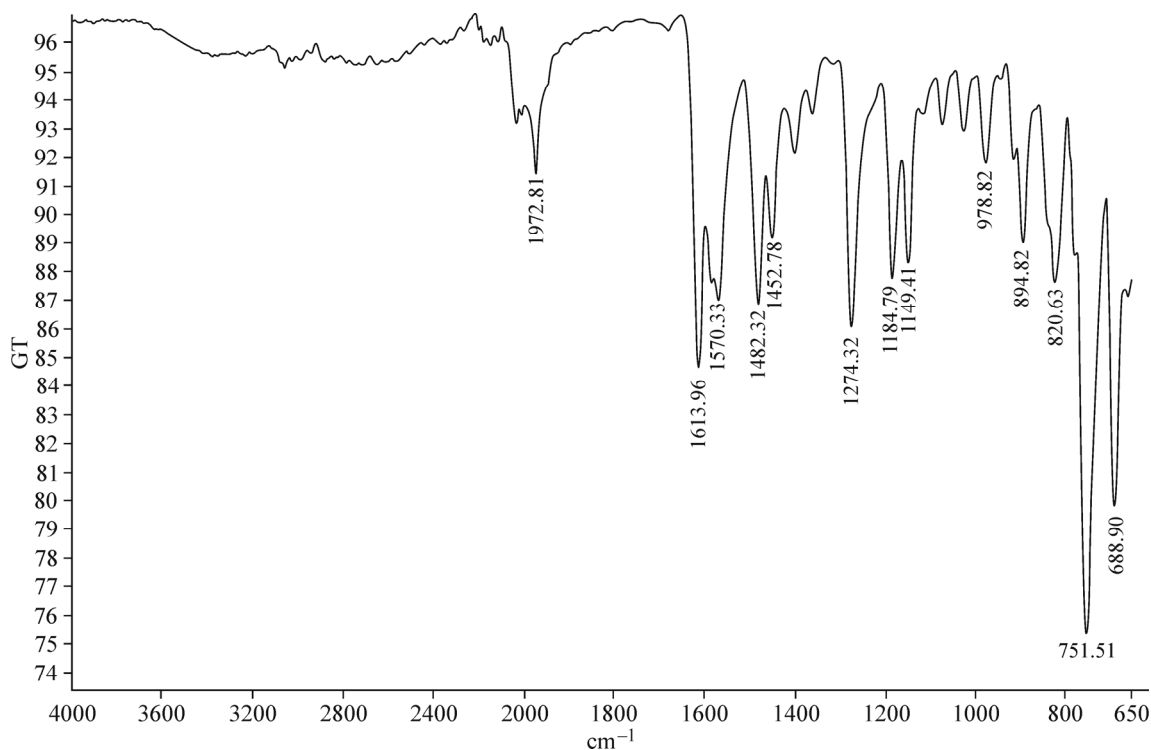
**Fig. 3.** FTIR spectrum of SA measured in the KBr pellet.
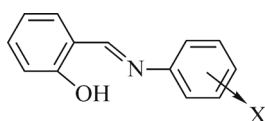
X= *o*- and *p*-NO$_2$, *o*- and *p*-Cl, *o*- and *p*-Br
X= *o*- and *p*-OCH$_3$, *o*- and *p*-NH$_2$, and *o*- and *p*-OH

Scheme 2. Series of substituted SA derivatives
studied in the present work.

Fig. 4 displays the electronic absorption spectra of the *o*-Cl, *o*-Br, and *o*-NO$_2$ SA derivatives, in both ethanol and cyclohexane as solvents. The general features of the spectra resemble those of the parent compound. The perturbation effect of the nitro group seems to be pronounced. Thus, a new absorption band appears at 375 nm ($\varepsilon = 3300$) while the second and
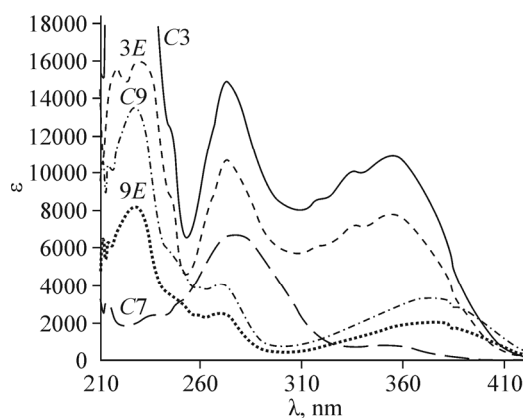

Fig. 4. Electronic absorption spectra of (3) *o*-Cl, (7) *o*-Br, and (9) *o*-NO$_2$ measured in cyclohexane (*C*) and ethanol (*E*) as solvents.

third transitions are now diffuse and appear as low intensity ($\varepsilon = 2700$) shoulders under the short wavelength tail of the new long wavelength band. The main configuration contributing to the first excited state is 63-64 configuration (0.7).

It is worth noting that the full geometry optimization of the *o*-nito derivative of SA at the B3LYB/611++G** level of theory reveals the non-coplanrity of the molecule. This is expected due the steric hindrance caused by the presence of a bulky NO_2 group in the *ortho* position. This steric hindrance forces the Ph–NO_2 moiety to be out-of-plane by an angle of 83°. The second order perturbation energy analysis of the *o*-NO_2 derivative (Table 2) reveals a dramatic change in the bonding as compared to parent SA. Thus, the interaction of the C_1–N_3 NBO with the π system of the nitrophenyl moiety is now reduced to very small values. The interaction of the C_1–N_3 NBO with the π system of the *o*-hydroxy phenyl moiety is more pronounced. One should also note that a pronounced interaction energy term between the C–N nitrogen lone pair orbital and the H25virtual orbital has been observed. Therefore, Table 2 and 4 data and the electronic spectra of the *o*-nitro phenyl derivative reveal that the charge redistributions might facilitate and lower the potential energy barrier for the proton transfer from the OH group to the nitrogen atom of the C–N group leading to a keto structure. There is also a reduction in the population of the NBO′s of the phenyl moiety due to the strong withdrawing effect of the nitro group.

Fig. 5 displays the optimized geometric structure of the *o*-nitro derivatives and some of the molecular orbitals involved in the electronic transitions. The first excited state is composed of one configuration 63-64. HOMO 63 is a delocalized MO (in spite of the non-coplanarity of the molecule) whereas LUMO 64 is localized over the Ph–OH moiety. Therefore, the long wavelength band is a $\pi\pi^*$ transition having a charge transfer character. The second and third excited states each involve three configurations; all involve the charge transfer to the Ph–OH moiety (Table 2). The electronic absorption spectrum of the *o*-Cl derivative of SA resembles to a great extent that of parent SA. However, all observed bands exhibit a marked increase in the intensity. This molecule demonstrates co-planarity. The general features of the spectrum of the *o*-Br derivative, on the other hand, are different. Thus, there is a considerable reduction in the intensity and a blue shift in the position of the long wavelength absorption band and a considerable intensification of the 275 nm band. The second and third bands (in the 320-290 nm region) are not observed in the spectrum of the *o*-Br derivative.

The vibrational spectrum of the *o*-NO_2 derivative of SA reflects the major geometry changes introduced by the nitro group. Thus, the *o*-NO_2 group seems to have a marked effect on SA IR marker bands. Thus, the OH stretching vibration is
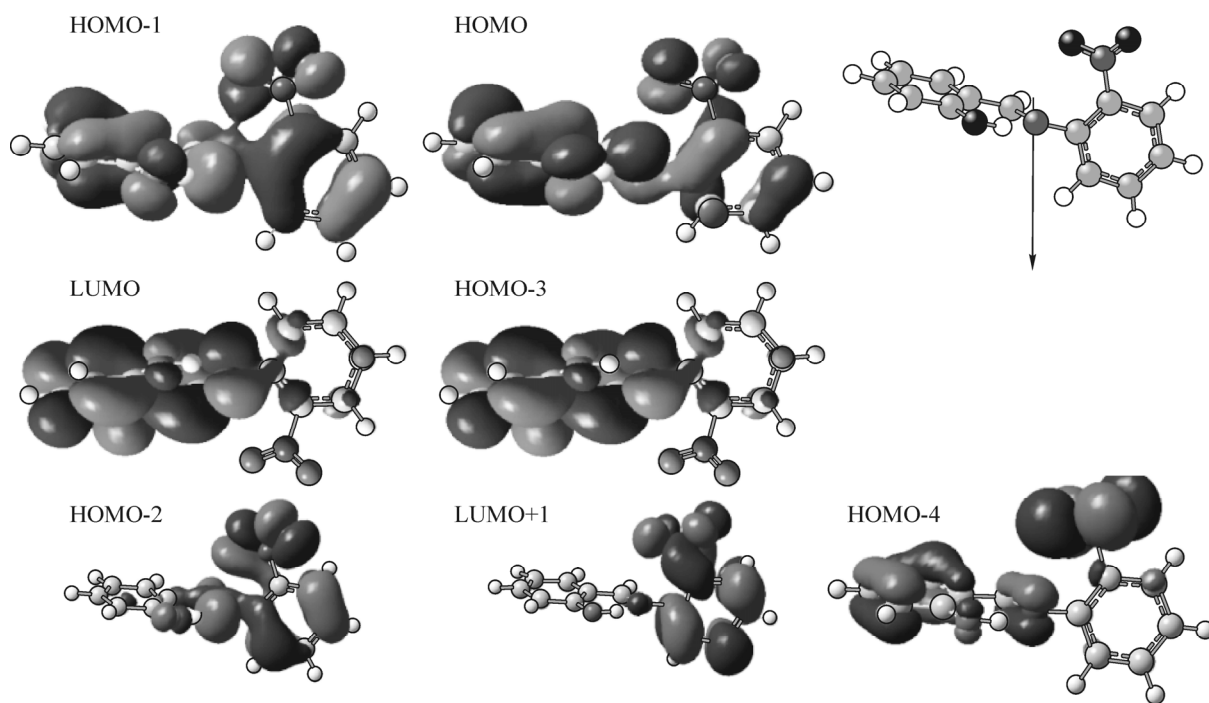
Fig. 5. Fully optimized geometry of the *o*-NO_2 derivative of SA and MOs involved in the electronic transitions.
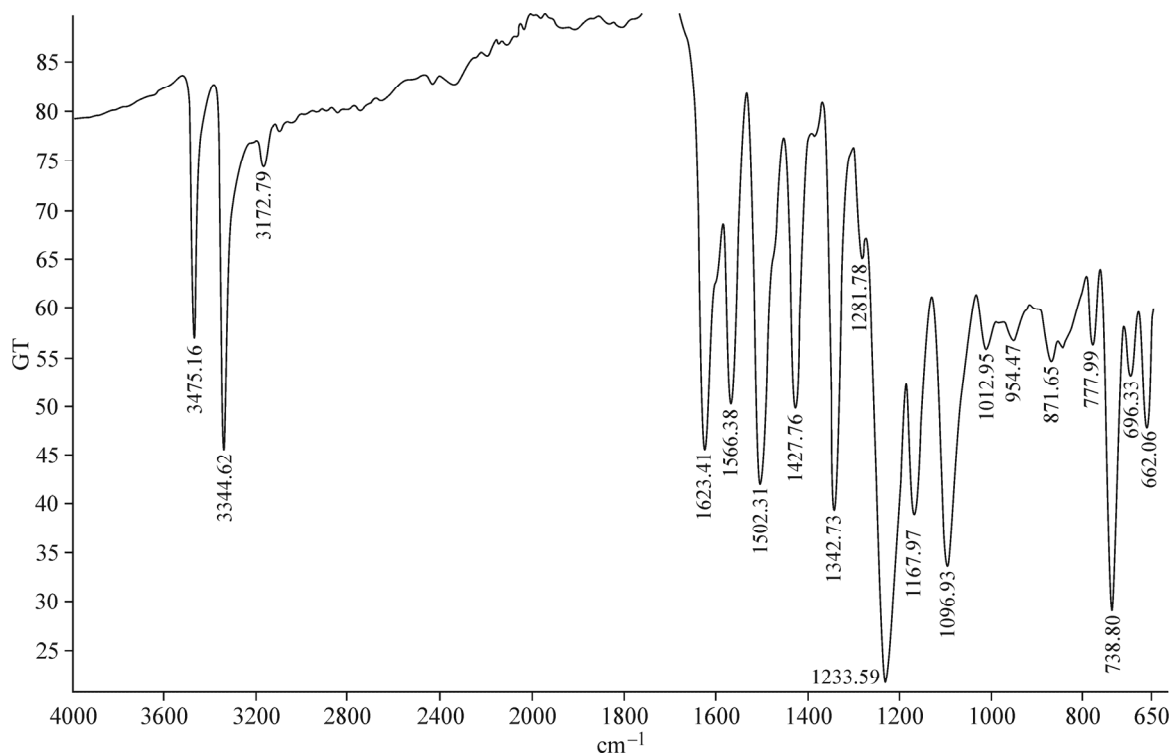
Fig. 6. FTIR spectrum of the *o*-Br derivative of SA measured in the KBr pellet.

shifted to 3316 cm^{-1} and is intensified. The C=N stretching mode suffers also the same trend where it is shifted to 1680 cm^{-1} and is considerably intensified. The C=N and phenyl ring breathing combination band shows also the same trend (Table 4). This same trend of shifting to higher wavenumbers and the intensification of the three IR marker bands are observed for *o*-Br and *o*-Cl derivatives. Fig. 6 displays the FTIR spectrum of the *o*-Br derivative of SA. The bulk *o*-Br group causes the splitting and intensification of the OH and aromatic CH stretching modes. These stretching bands are also shifted to longer wavenumber values.

In conclusion, the substitution in the *ortho* position of the N–Ph moiety by electron withdrawing substituents such as NO$_2$, Cl, and Br causes non-coplanarity of the SA molecular skeletal structure and all observed $\pi\pi^*$ transitions have a considerable charge transfer character in the direction of the Ph–NO$_2$ moiety. However, these types of substitution do not in general create new transitions, except the case of the NO$_2$ derivative where a long wavelength band at 380 nm is observed. Furthermore, electron withdrawing groups in the *ortho* position also have the general effect of shifting the IR marker bands of SA to higher wavenumbers and appreciably increase their intensities.

The substitution by the same electron withdrawing groups but in the *para*-position of the N–Ph moiety does not introduce as much perturbation as that observed in the case of *ortho* substitution (Table 3). Thus, the *p*-NO$_2$ derivative is still non-coplanar, but the dihedral angle between the plane of the Ph–NO$_2$ moiety and the rest of the molecule is much smaller (38°) than that in the case of the *o*-NO$_2$ derivative. The origin of the non-coplanarity in the case of the *para* derivative is the dimensioned charge density accumulation in the NO$_2$Ph–N bond region. The NO$_2$ group acts as an electron sink withdrawing the charge density away from this region. NBO analysis of the *p*-NO$_2$ derivative (Table 2) indicates that it retained the extended conjugation of SA as revealed by the interaction of C$_1$–N$_3$ NBOs with those of both phenyl rings. Furthermore, the interaction of the nitrogen lone orbitals with the hydroxyl group hydrogen atom is marked. Table 3 data indicate that the electronic spectrum, however, resembles to a great extent that of the *ortho* derivative yet more diffuse and of a lower intensity. The *p*-Br substitution causes a marked red shift of the first absorption band to 356 nm whilst the second and third bands appear overlapping with the peak maxima at 328 nm and 312 nm. One should note that the band appearing at 270 nm in SA seems to be persistent and appears in almost the same region in all derivatives studied. This band is a conjugation band characterizing the SA π framework.

TABLE 3. Experimentally Observed and Theoretically Computed Electronic Spectral Characteristics of SA Derivatives Studied in the Present Work

Com-pounds	Molecular orbital contribution	λ, nm	f	λ$_e$	λ$_c$	Com-pounds	Molecular orbital contribution	λ, nm	f	λ$_e$	λ$_c$
	Theoretical			**Experimental**			**Theoretical**			**Experimental**	
2	H→L	0.69964	385	0.3	362	366	8	H→L	0.67771	360	0.43	346	347
	H-4→L	0.62101	332	0.01				H-1→L	0.66816	313	0.47	331	
	H-1→L	0.6778	329	0.5	318	319		H-4→L+1	0.70268	290	0.0001		
	H-1→L+1	0.63103	310	0.02				H→L+1	0.47585	279	0.01		
	H-2→L+1	0.49278	295	0.04	227	228		H-3→L+1	0.56654	258	0.01	267	266
	H-3→L+1	0.57715	290	0.01	219	220		H→L+2	0.49281	254	0.07	230	231
3					385	355	9	H→L	0.69784	381	0.01	371	372
					354	334		H-1→L	0.60003	346	0.043		
	H→L	0.66692	334	0.30	333	232		H→L+1	0.63254	320	0.13		
	H-1→L	0.66105	316	0.01				H-3→L	0.44848	319	0.003		
	H-2→L	0.62149	279	0.01	272	272		H-2→L	0.6417	307	0.003		
	H-3→L	0.57736	261	0.30				H-2→L+1	0.66115	303	0.015		
	H→L+1	0.63134	253	0.02								267	269
	H-1→L+1	0.57893	239	0.02	228	229						225	227
4	H→L	0.69393	354	0.60	385	359	10	H→L	0.67988	349	0.33	359	369
	H-1→L	0.68269	318	0.04	334	333		H-2→L	0.69732	323	0.0001	334	335
	H→L+2	0.54786	279	0.02				H-1→L	0.66737	298	0.50		
	H-4→L	0.46621	270	0.20	270	272		H-3→L	0.55166	279	0.002		
	H-4→L	0.43115	255	0.01	293	296		H→L+1	0.57345	254	0.04	263	265
	H-3→L	0.5335	252	0.05	224	227		H-5→L	0.66735	248	0.00		227
5	H→L	0.6889	349	0.40	349	353	11	H→L	0.69666	372	0.75	364	365
	H-1→L	0.68264	320	0.01	329			H-1→L	0.67978	322	0.05	326	
	H-2→L	0.59137	290	0.02				H→L+1	0.63693	294	0.04		
	H-3→L	0.54747	270	0.30	269	270		H-4→L	0.70233	284	0.0001		
	H→L+1	0.60048	252	0.02				H→L+2	0.69382	278	0.002		
	H→L+2	0.58548	243	0.09	225	228		H→L+3	0.53052	267	0.04	265	266
6	H→L	0.67877	361	0.46	353	355						229	230
	H-1→L	0.67028	316	0.45	328	329	12	H→L	0.67693	349	0.39		
	H-4→L	0.70143	291	0.001	310	313		H-1→L	0.64759	307	0.26		
	H→L+1	0.4764	280	0.01	272	273		H-2→L	0.61882	285	0.24		
	H-2→L	0.55738	262	0.04				H-3→L	0.70225	292	0.00		
	H→L+1	0.50277	254	0.07	230	232		H→L+1	0.58127	256	0.03	265	266
7	H→L	0.68297	357	0.31	345	350		H→L+2	0.67465	251	0.001	252	
	H-3→L	0.69869	306	0.0001								223	224
	H-1→L	0.66536	305	0.50									
	H-2→L	0.62409	291	0.08									
	H→L+2	0.66453	263	0.46	275	277							
	H→L+1	0.64169	259	0.05	233	234							

* Only main configurations.
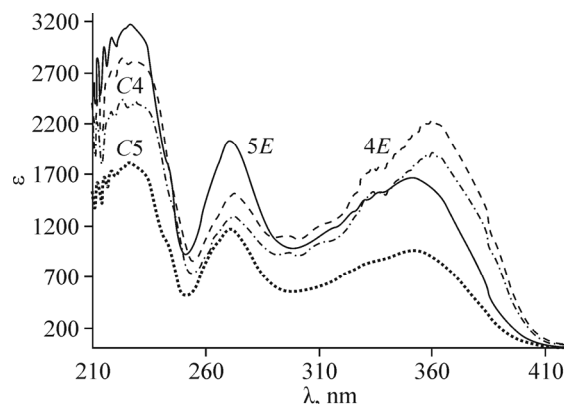
Fig. 7. Electronic absorption spectra of the (4) -*o*-OCH₃ and (5) *p*-OCH₃ SA derivatives measured in cyclohexane (*C*) and ethanol (*E*) as solvents.

Electron withdrawing substituents in the *para* position do not have the same marked effect noted in the case of the *ortho* substitution. In fact, the IR marker bands do not show any significant shift in peak positions. However, peak intensities show a reduction in intensities. Nevertheless, the main observation to be made here is the coupling between the OH and aromatic CH stretching modes with a consequent reduction in the intensity.

Fig. 7 displays the electronic absorption spectra of the *o*-OCH₃ and *p*-OCH₃ derivatives of SA in cyclohexane and ethanol as solvents. Electron donating groups cause a marked shift of the electron density onto the –N=C–phenol moiety. The *o*-methoxy substitution forces the N–Ph moiety out of the plane of the molecule; the dihedral angle is 38°. However, the general features of the spectrum of SA is unaffected by the *o*-OCH₃ substitution. The first absorption band is slightly red shifted and all observed bands suffer a reduction in the intensity. The first absorption band observed at 358 nm and predicted theoretically at 360 nm are in excellent agreement. Two configurations contribute to this S_1 state, with 69-70 (0.7) as the main configuration. Thus, as Table 3 indicates, this transition corresponds to a ππ* state delocalized over the entire molecule. The *o*-NH₂ substitution causes not only a red shift of the observed transitions but also the intensification, especially for the second absorption band that became more intense than the first. This band seems to be more affected by the substitution. In the case of the *o*-OH derivative (Table 3), this band is red shifted to the extent that it became obscured under the broad long wavelength band.

Inspection of Fig. 7 and Table 3 clearly indicates that the general features of the spectra of the *para* substituted derivatives are essentially the same as those of the corresponding *ortho* derivatives. In general, the electron donating substitution causes a red shift and the intensification of the observed transitions. The second absorption band originally appearing at 320 nm is most affected by the substitution. It is a red shift to 340 nm and may become obscured by the broad long wavelength band. It is interesting to note that the hydroxyl group substitution either in the *ortho* or *para* positions causes the coupling of the C–N stretching mode with the asymmetric aromatic C=C stretching and OH bending modes. These two coupling modes appear at 1660 cm⁻¹ and 1608 cm⁻¹. The two OH groups, on the other hand, do not couple with each other and appear at 3800 cm⁻¹ and 3210 cm⁻¹ (Table 4).

CONCLUSIONS

The present experimental and DFT/TDDFT investigations of the electronic structure and spectra of SA and some of its derivatives reveal that SA enjoys linear conjugation which is responsible for the observed spectrum. No specific part of the molecule reflects itself in the observed spectrum due to the extended π system. The interaction between the oxygen and hydrogen atomic orbitals is of a covalent character, and thus, a proton transfer toward the nitrogen atom in the ground state would be opposed by a high energy barrier. A set of 12 substituted SA derivatives has been investigated. The choice of these substituents aims to create a push-pull system on the SA basic structure, which would shade light onto its photo physics. The

TABLE 4. Experimentally Observed and Theoretically Computed Vibrational Spectral Characteristics and Assignments of IR Marker Bands of SA and Some of its Derivatives

Compound	ν_{exp}, cm^{-1}	ν_{calc}, cm^{-1}	Relative intensity	Assignment
SA	3600-2800(w)	3175	334	OH str.
	1613(s)	1663, 1660	43, 160	C=N str., C=Nstr+OH bending
		1606	140	C=N str.+ring breathing vibration
	751 (vs)	859	8.9	
p-NO$_2$	3600-2800(w)	3276	514	OH str.
	1599 (s)	1664	212	C=N
	1561(s)	1660	383	C=Nstr.+OH bending
	759 (vs)	790	5	C=Nstr.+ring breathing
o-Cl	3600-2800 (w)	3252	575	OH str.
	1608(s)	1670	362	C=N str.
		918	36	C=Nstr.+ring breathing
p-OCH$_3$	3600-2800 (w)	3203	507	OH str.
	1608 (s)	1664	316	C=Nstr. Coupled with ring modes
	833 (vs)	919	15	C=Nstr.+ring breathing
o-OH	3600-2800 (w)	3120	452	OH str.
		3800	48	OH str. (salisaylidene)
	1613 (s)	1660	156	C=N str. Coupled with ring modes
	1590 (s)	1608	143	C=Nstr.+OH bending
	736 (vs)	854	25	C=N Str.+ring breathing
p-Br	3600-3200 (s)	3197	280	OHstr. Coupled with arom.CH
	1606 (s)	1659	287	C=Nstr.
	828 (vs)	792	7	C=Nstr.+ring breathing
o-Br	3600-3200 (w)	3156	370	OHstr.
		3136	72	OHstr.Coupled with.CH(C=N)
	1611(s)	1656	242	C=Nstr.
	1185 (s)	1000	172	C=Nstr. Oupled with OH bending
	752 (vs)	865	14	C=Nstr.+ring breathing
p-Cl	3059 (s)	3200	170	OHstr. +arom.CH
	2938 (s)	3190	148	OHstr.+arom.CH
	1615 (w)	1665	716	C=N str.
	744 (vs)	780	19	C=Nstr.+ring breathing
o-NO$_2$	3375 (w)	3316	600	OHstr.
	3344 (w)		541	C=Nstr.
	1623 (s)	1680	32.4	C=Nstr.+ring breathing
	738	845		
p-OH	3389 (s)	3835	107	OH str.
	3300(w)	3206	494	OH str. (salisaylidene)
	1612(w)	1665	300	C=N str. Coupled with ring modes
	835 (vs)	871	8.7	C=N Str.+ring breathing

substitution by bulky groups in the *ortho* position of the N–Ph moiety forces it out of the plane of the molecules, yet the π conjugation and hyperconjugation across the C=N bond minimized the effect of non-coplanarity on the observed spectrum. The observed transitions are sensitive to both solvent and substituent effects. The extent of the charge transfer character and

its direction enabled the interpretation of the observed shifts in band positions and intensities. The analysis of the experimentally determined and theoretically computed FTIR spectra of SA enabled the identification of three "IR marker bands", namely, the OH stretching mode at 3175 cm^{-1}, the C=N stretching mode at 1660 cm^{-1}, and the C=N and ring breathing combination band at 850 cm^{-1}. These bands are persistent in all substituted SAs studied in the present work and are sensitive to the type and position of the substitution.

REFERENCES

1. G. O. Dudek and E. P. Dudek, *J. Am. Chem. Soc.*, **88**, 2407 (1966).
2. T. Rosenfeld, M. Ottolenghi, and A. Y. Meyer, *Mol. Photochem.*, **5,** 39 (1973).
3. J. W. Lewis and C. Sandorfy, *Can. J. Chem.*, **60,** 1727 (1982).
4. R. S. Becker, C. Lenoble, and A. Zein, *J. Phys. Chem.*, **91,** 3509 (1987).
5. T. Elsässer and H. J. Bakker, *Ultrafast Hydrogen Bonding Dynamics and Proton Transfer Processes in the Condensed Phase*, Kluwer Academic Publ. (2002).
6. E. Hadjoudis and I. M Mavridis., *Chem. Soc. Rev.*, **33**, 579 (2004).
7. M. Irie, *Chem. Rev.*, **100,** 1685 (2000).
8. V. Vargas and L. Amigo, *J. Chem. Soc.*, *Perkin Trans. 2,* 1124 (2001).
9. T. Dziembowska, E. Jagodzińska, Z. Rozwadowski, and M. Kotfica, *J. Mol. Struct.*, **598**, 229 (2001).
10. K. Ogawa, J. Harada J., T. Fujiwara, and S. Yoshida, *J. Phys. Chem. A*, **105,** 3425 (2001).
11. A. Mandal, D. Fitzmaurice, E. Waghorne, A. Koll, A. Filarowski, D. Guha, and S. Mukherjee, *J. Photochem. Photobiol., A*, **153,** 67 (2002).
12. M. Rospenk, I. Król-Starzomska, A. Filarowski, and A. Koll, *Chem. Phys.*, **287**, 113 (2003).
13. A. Ohshima, A. Momotake, and T. Arai, *J. Photochem. Photobiol., A,* **162,** 473 (2004).
14. W. M. Fabian, L. Antonov, D. Nedeltcheva, F. S. Kamounah, and P. J. Taylor, *J. Phys. Chem. A,* **108,** 7603 (2004).
15. P. Barbara, P. Rentzepis, and L. Brus, *J. Am. Chem. Soc.*, **102,** 2786 (1980).
16. K. Kownacki, A. Mordzinski, R. Wilbrandt, and A. Grabowska, *Chem. Phys. Lett.*, **227,** 270 (1994).
17. A. Grabowska and K. Kownacki, *J. Lumin.*, **60,** 886 (1994).
18. M. Z. Zgierski and A. Grabowska, *J. Chem. Phys.*, **112,** 6329 (2000).
19. M. Knyazhansky, A. Metelitsa, M. Kletskii, A. Millov, and S. Besugliy, *J. Mol. Struct.*, **526,** 65 (2000).
20. H. Joshi, F. S. Kamounah, C. Gooijer, G. van der Zwan, and L. Antonov, *J. Photochem. Photobiol., A*, **152,** 183 (2002).
21. N. Otsubo, C. Okabe, H. Mori, K. Sakota, K. Amimoto, T. Kawato, and H. Sekiya, *J. Photochem. Photobiol., A*, **154,** 33 (2002).
22. S. Mitra and N. Tamai, *Phys. Chem. Chem. Phys.*, **5,** 4647 (2003).
23. M. Ziółe, J. Kubicki, A. Maciejewski, R. Naskręcki, and A. Grabowska, *Phys. Chem. Chem. Phys.*, **6,** 4682 (2004).
24. C. Okabe, T. Nakabayashi, Y. Inokuchi, N. Nishi, and H. Sekiya, *J. Chem. Phys.*, **121,** 9436 (2004).
25. S. Mitra and N. Tamai, *Chem. Phys. Lett.*, **282,** 391 (1998).
26. S. Mitra and N. Tamai, *Chem. Phys.*, **246,** 463 (1999).
27. V. Vargas, *J. Phys. Chem. A*, **108,** 281 (2004).
28. Rodríguez-Córdoba, W. J. S. Zugazagoitia, E. Collado-Fregoso, and J. Peon, *J. Phys. Chem. A*, **111,** 6241 (2007).
29. M. Ziółek, J. Kubicki, A. Maciejewski, R. Naskr□cki, and A. Grabowska, *J. Chem. Phys.*, **124,** 124518 (2006).
30. G. W. T. M. J. Frisch, H. B. Schlegel, G. E. Scuseria, M. A. Robb, J. R. Cheeseman, G. Scalmani, V. Barone, B. Mennucci, G. A. Petersson, H. Nakatsuji, M. Caricato, X. Li, H. P. Hratchian, A. F. Izmaylov, J. Bloino, G. Zheng, J. L. Sonnenberg, M. Hada, M. Ehara, K. Toyota, R. Fukuda, J. Hasegawa, M. Ishida, T. Nakajima, Y. Honda, O. Kitao, H. Nakai, T. Vreven, J. A. Montgomery Jr., J. E. Peralta, F. Ogliaro, M. Bearpark, J. J. Heyd, E. Brothers, K. N. Kudin, V. N. Staroverov, R. Kobayashi, J. Normand, K. Raghavachari, A. Rendell, J. C. Burant, S. S. Iyengar, J. Tomasi,

M. Cossi, N. Rega, J. M. Millam, M. Klene, J. E. Knox, J. B. Cross, V. Bakken, C. Adamo, J. Jaramillo, R. Gomperts, R. E. Stratmann, O. Yazyev, A. J. Austin, R. Cammi, C. Pomelli, J. W. Ochterski, R. L. Martin, K. Morokuma, V. G. Zakrzewski, G. A. Voth, P. Salvador, J. J. Dannenberg, S. Dapprich, A. D. Daniels, O. Farkas, J. B. Foresman, J. V. Ortiz, J. Cioslowski, and D. J. Fox, *Gaussian Inc*., Wallingford, CT (2009).

31. T. Schaefer, T. A. Wildman, and S. R. Salman, *J. Am. Chem. Soc*., **102,** 107 (1980).
32. T. Schaefer, S. R. Salman, T. A. Wildman, and P. D. Clark, *Can. J. Chem.*, **60,** 342 (1982).
33. A. D. Becke, *J. Chem. Phys.*, **98,** 5648 (1993).
34. R. Bauernschmitt and R. Ahlrichs, *Chem. Phys. Lett.*, **256,** 454 (1996).
35. S. E. Ulic, C. O. D. Védova, A. Hermann, H.-G. Mack, and H. Oberhammer, *J. Phys. Chem. A,* **112,** 6211 (2008).
36. A. E. Reed and F. Weinhold, *J. Chem. Phys*., **78,** 4066 (1983).
37. X. Chen, F. Yan, M. Wu, H.-B. Tian, S. X. Li, X. Shan, K. Wang, Z. Li, and K. Xu, *Chem. Phys. Lett.*, **472,** 19 (2009).
38. H. P. H. Frisch, A. E…….., R. D. Dennington II, et al., *Gaussian Inc*., Wallingford, CT (2009), p. 235.